

Dynamics of Atom-Mediated Photon-Photon Scattering I: Theory

M. W. Mitchell and R. Y. Chiao

Department of Physics, University of California at Berkeley, Berkeley, CA 94720, USA

(November 11, 2018)

The mediated photon-photon interaction due to the resonant Kerr nonlinearity in an inhomogeneously broadened atomic vapor is considered. The time-scale for photon-photon scattering is computed and found to be determined by the inhomogeneous broadening and the magnitude of the momentum transfer. This time can be shorter than the atomic relaxation time. Effects of atom statistics are included and the special case of small-angle scattering is considered. In the latter case the time-scale of the nonlinear response remains fast, even though the linear response slows as the inverse of the momentum transfer.

I. INTRODUCTION

Recently there has been experimental and theoretical interest in the nonlinear optics of confined light [1]. A medium possessing an optical Kerr nonlinearity and confined within a planar or cylindrical Fabry-Perot resonator gives rise to new nonlinear optical phenomena such as soliton filtering and bilateral symmetry breaking [2,3]. The classical nonlinear optics of this system is described by the Complex Ginzburg-Landau equation (CGLE)

$$\frac{\partial E}{\partial t} = \frac{ic}{2n_0k} \nabla_{\perp}^2 E + i\omega A \frac{n_2}{n_0} |E|^2 E + \frac{ic\Delta k}{n_0} E - \Gamma(E - E_d), \quad (1)$$

where E is the electric field envelope, k is the longitudinal wavenumber, $\omega = ck/n_0$ is the field envelope angular frequency, A is a mode overlap factor, Δk is the wavenumber mismatch from the linear-cavity response and Γ is the field amplitude decay rate. The classical dynamics of Eq. (1) describes the mean-field behavior of a system of interacting photons coherently coupled to an external reservoir. A photonic system of this sort is a versatile model system for condensed matter physics in reduced dimensions [4], as the parameters $\Delta k, n_2, \Gamma$, and E_d in Eq. (1) are subject to experimental control. In particular, an atomic vapor can provide a strong Kerr nonlinearity which is tunable both in strength and in sign. In this case the nonlinearity arises from the saturation of the linear refractive index, which is a strong function of the drive laser frequency near an absorption resonance.

Some of the most interesting proposed experiments for this system, including generation of few-photon bound states [5], direct observation of the the Kosterlitz-Thouless transition in an optical system [4] and observation of quantum corrections to the elementary excitation spectrum of a 1D photon gas [6,7] intrinsically involve photon correlations. For this reason, it is important to understand the microscopic (and not just mean-field) behavior of photons in an optical Kerr medium. We specifically consider saturation of the resonant electronic polarization of a Doppler-broadened atomic vapor, a medium

which has been proposed for quantum cavity nonlinear optics experiments and used to observe a nonlinear cavity mode [2]. Thus the system under consideration involves dispersion, loss, inhomogeneous broadening, and the continuum of transverse modes in an extended resonator.

Sophisticated techniques have been developed for treating mediated interactions among photons in nonlinear media. One approach is to obtain an effective theory in which the quanta are excitations of coupled radiation-matter modes, by canonical quantization of the macroscopic field equations [8,9], or by direct attack on a microscopic Hamiltonian [10]. This approach has the advantage of generality and is suited to multi-mode problems, but has basic difficulties with loss and dispersion near resonance [11–13]. Microscopic treatments include Scully-Lamb type theory [14,15] and application of phase-space methods [16,17]. A strength of these techniques is their ability to handle relaxation and population changes. They are, however, cumbersome to apply to inhomogeneously broadened media and to multi-mode problems.

In this paper we characterize the atom-mediated photon-photon interaction using an accurate microscopic model and perturbation calculations. This allows us to determine the time-scale of the mediated photon-photon interaction in the atomic vapor, despite the complexity of the medium. We find that the interaction is fast and not intrinsically lossy, even for small momentum transfer. Thus the medium is suitable for quantum optical experiments, including experiments using the NLFP as a model for the interacting Bose gas.

II. SCATTERING CALCULATIONS

The complete system is treated as the quantized electromagnetic field interacting via the dipole interaction with an vapor of atoms of mass M . The perturbation calculations are performed in momentum space, as is natural for thermodynamic description of the atomic vapor. This also makes simple the inclusion of atomic recoil effects. The dipole interaction term is identified as the

perturbation, so that the eigenstates of the unperturbed Hamiltonian are direct products of Fock states for each field. In the rotating wave approximation, the unperturbed and perturbation Hamiltonians are

$$H_0 = \sum_{\mathbf{k}, \alpha} \hbar c k a_{\mathbf{k}, \alpha}^\dagger a_{\mathbf{k}, \alpha} + \sum_{n, \mathbf{p}} (\hbar \omega_n + \frac{\hbar^2 \mathbf{p}^2}{2M}) c_{n, \mathbf{p}}^\dagger c_{n, \mathbf{p}} \quad (2)$$

$$\begin{aligned} H' &= -\mathbf{E}(\mathbf{x}) \cdot \mathbf{d}(\mathbf{x}) \\ &= -\sum_{\mathbf{k}, \alpha} \sqrt{\frac{2\pi \hbar c k}{V}} \sum_{n, m, \mathbf{p}} i \mathbf{e}_{\mathbf{k}, \alpha} \cdot \boldsymbol{\mu}_{nm} c_{n, \mathbf{p}+\mathbf{k}}^\dagger c_{m, \mathbf{p}} a_{\mathbf{k}, \alpha} \\ &\quad + \text{h.c.} \end{aligned} \quad (3)$$

where $a_{\mathbf{k}, \alpha}$ is the annihilation operator for a photon of momentum $\hbar \mathbf{k}$ and polarization α , $c_{n, \mathbf{p}}$ is the annihilation operator for an atom in internal state n with center-of-mass momentum $\hbar \mathbf{p}$, \mathbf{E} is the quantized electric field and \mathbf{d} is the atomic dipole field. Polarization plays only a very minor role in this discussion so polarization indices will be omitted from this point forward.

The simplest mediated interaction is photon-photon scattering, which transfers momentum from one photon to another by temporarily depositing this momentum in the medium. Specifically, photons with momenta \mathbf{k}, \mathbf{l} are consumed and photons with momenta $\mathbf{k}' \equiv \mathbf{k} + \mathbf{q}, \mathbf{l}' \equiv \mathbf{l} - \mathbf{q}$ are produced. The lowest-order processes to do this are fourth order, so we look for relevant terms in $H'H'H'H'$. A parametric process, i.e., one which leaves the medium unchanged, sums coherently over all atoms which could be involved [18]. Due to this coherence, the rates of parametric processes scale as the square of N/V , the number density of atoms. In contrast, incoherent loss processes such as Rayleigh and Raman scattering scale as N/V . Thus for large atomic densities, a given photon is more likely to interact with another photon than it is to be lost from the system.

In this sense, the interaction is not intrinsically lossy, as are some optical Kerr nonlinearities such as optical pumping or thermal blooming. The latter processes require absorption of photons before there is any effect on other photons. For this reason, they are unsuitable for quantum optical experiments such as creation of a two-photon bound state.

One parametric process, photon-photon scattering at a single atom, is described by the diagram of Fig. 1. The relevant terms in $H'H'H'H'$ contain

$$\begin{aligned} &c_{a, \mathbf{p}}^\dagger c_{d, \mathbf{p}+\mathbf{l}'} a_{\mathbf{l}'}^\dagger c_{d, \mathbf{p}+\mathbf{l}}^\dagger c_{c, \mathbf{p}-\mathbf{q}} a_{\mathbf{l}} \\ &\times c_{c, \mathbf{p}-\mathbf{q}}^\dagger c_{b, \mathbf{p}+\mathbf{k}} a_{\mathbf{k}}^\dagger c_{b, \mathbf{p}+\mathbf{k}}^\dagger c_{a, \mathbf{p}} a_{\mathbf{k}} \end{aligned} \quad (4)$$

or permutations $\mathbf{k}' \leftrightarrow \mathbf{l}'$, $\mathbf{k} \leftrightarrow \mathbf{l}$ for a total of four terms. Here \mathbf{p} is the initial atomic momentum and a through d index the atomic states involved. With the assumption that no atoms are initially found in the upper states b and d , i.e., $n_b = n_d = 0$, this reduces to

$$n_{a, \mathbf{p}} (1 \pm n_{c, \mathbf{p}-\mathbf{q}}) a_{\mathbf{l}'}^\dagger a_{\mathbf{l}} a_{\mathbf{k}}^\dagger a_{\mathbf{k}} \quad (5)$$

where the n are number operators for the atomic modes and the upper and lower signs hold for Bose and Fermi gases, respectively. The difference for atoms of different statistics reflects the fact that the scattering process takes the atom through an intermediate momentum state which could be occupied. Occupation of this intermediate state enhances the process for Bose gases but suppresses it for Fermi gases.

A thermal average of the relevant terms in $H'H'H'H'$ gives the thermally averaged effective perturbation

$$\langle H'_{\text{eff}} \rangle = \frac{(2\pi)^3}{V} \sum_{\mathbf{k} \mathbf{l} \mathbf{l}'} V_{\mathbf{l}' \mathbf{k}' \mathbf{l} \mathbf{k}} a_{\mathbf{l}'}^\dagger a_{\mathbf{l}} a_{\mathbf{k}}^\dagger a_{\mathbf{k}} \quad (6)$$

where

$$V_{\mathbf{l}' \mathbf{k}' \mathbf{l} \mathbf{k}} \equiv \sum_a \int d^3 \mathbf{p} v_{\text{eff}}(\mathbf{p}, a, c) \langle n_{a, \mathbf{p}} \rangle \sum_c (1 \pm \langle n_{c, \mathbf{p}-\mathbf{q}} \rangle), \quad (7)$$

$$v_{\text{eff}}(\mathbf{p}, a, c) = v_{\text{eff}}^{(1)} + v_{\text{eff}}^{(2)} + v_{\text{eff}}^{(3)} + v_{\text{eff}}^{(4)} \quad (8)$$

$$\begin{aligned} v_{\text{eff}}^{(1)} &= \frac{c^2 \sqrt{k l k' l'}}{(2\pi)^4 \hbar} \\ &\times \sum_{bd} (\mathbf{e}_{\mathbf{l}'} \cdot \boldsymbol{\mu}_{da})^* \mathbf{e}_{\mathbf{l}} \cdot \boldsymbol{\mu}_{dc} (\mathbf{e}_{\mathbf{k}'} \cdot \boldsymbol{\mu}_{bc})^* \mathbf{e}_{\mathbf{k}} \cdot \boldsymbol{\mu}_{ba} \\ &\times [R_1^{(1)} R_2^{(1)} R_3^{(1)}]^{-1} \end{aligned} \quad (9)$$

and similar expressions obtain for $v_{\text{eff}}^{(2-4)}$. and $\langle n_{a, \mathbf{p}} \rangle$ is the average occupancy of the atomic state $|a, \mathbf{p}\rangle$. The $R_i^{(1)}$ are the resonance denominators

$$\begin{aligned} R_1^{(1)} &= c(k + l - k') - \frac{\hbar}{M} [\mathbf{p} \cdot \mathbf{l}' + l'^2/2] - \omega_{da} + i\gamma_d \\ R_2^{(1)} &= c(k - k') - \frac{\hbar}{M} [-\mathbf{p} \cdot \mathbf{q} + q^2/2] - \omega_{ca} + i\eta \\ R_3^{(1)} &= c(k) - \frac{\hbar}{M} [\mathbf{p} \cdot \mathbf{k} + k^2/2] - \omega_{ba} + i\gamma_b. \end{aligned} \quad (10)$$

Here $\hbar \omega_{ij} \equiv \hbar(\omega_i - \omega_j)$ is the energy difference between states i and j , γ_i is the inverse lifetime of state i and η is a vanishing positive quantity. Here and throughout, the process is understood to conserve photon momentum, but for clarity of presentation this is not explicitly indicated.

As described in Appendix A, intensity correlation functions for photon-photon scattering products contain a Fourier transform of the scattering amplitudes

$$P(x_A, t_A, x_B, t_B) \propto \left| \int d\delta k' V_{\mathbf{l}' \mathbf{k}' \mathbf{l}_0 \mathbf{k}_0} \exp[i c \delta k' \tau_-] \right|^2 \quad (11)$$

where $\delta k'$ is the output photon energy shift, $x_{A,B}$ and $t_{A,B}$ are detection positions and times, respectively, and $\tau_- \equiv t_B - x_B/c - t_A + x_A/c$ is the difference in retarded times. This expression allows us to determine the time correlations for photon-photon scattering in a number of important cases.

III. LARGE-ANGLE SCATTERING

The simplest configuration to understand is that of counterpropagating input beams producing counterpropagating output photons scattered at large angles. This is also the most convenient experimental geometry.

A. One Atom Process

Scattering amplitudes and rates for right-angle scattering by the one-atom process are shown in Fig. 2 and Fig. 3, respectively. For the moment we ignore the statistical correction due to the $n_{a,\mathbf{p}}n_{c,\mathbf{p}-\mathbf{q}}$ term in Eq. (7), which will be considered separately. The vapor is treated as a gas of two-level atoms. The parameters are the Doppler width $\delta_D \equiv k(k_B T/M)^{1/2}$, where k_B is Boltzmann's constant, the radiative linewidth $\gamma_b = A_E/2$ where A_E is the Einstein A coefficient, and the detuning $\Delta \equiv ck - \omega_{ba}$, in the ratios $\gamma_b = 0.01\delta_D$, $\Delta = 2\pi\delta_D$. The amplitude units are arbitrary, but do not vary between graphs.

At this point it is important to note that the duration of the correlation signal is much shorter than the coherence lifetime of an individual atom, approximately γ_b^{-1} . In fact, the duration of the correlation signal is determined by the momentum distribution, a property of the medium as a whole. This can be explained in terms of the coherent summation of amplitudes for scattering processes occurring at different atoms. The process is coherent only when it is not possible, even in principle, to tell which atom participated. This clearly requires momentum conservation among the photons, but it also limits the duration of the atomic involvement. An atom acting as intermediary to transfer momentum \mathbf{q} is displaced during the time it remains in the state c of Fig. 1. If this displacement is larger than the thermal deBroglie wavelength Λ it is possible, in principle, to determine which atom participated. This limits the duration of the coherent process to $\delta\tau \sim \Lambda M/\hbar q$.

B. Statistical Correction

As noted above, the quantum statistics of the atoms in the vapor contribute a correction to the single-atom scattering amplitude. This correction (with the sign appropriate for Bose atoms) is shown in Fig. 4 for a gas with phase space density $N\Lambda^3/V = 1/2$, where

$\Lambda \equiv (Mk_B T/2\pi\hbar^2)^{1/2}$ is the thermal deBroglie wavelength. Parameters are as for Fig. 2.

C. Simultaneous scattering

A second parametric process, simultaneous scattering, is described by the diagram of Fig. 5. The relevant terms in $H'H'H'H'$ contain

$$c_{a,\mathbf{p}}^\dagger c_{d,\mathbf{p}+\mathbf{l}'} a_{\mathbf{l}'}^\dagger c_{c,\mathbf{p}-\mathbf{q}}^\dagger c_{b,\mathbf{p}+\mathbf{k}} a_{\mathbf{k}'}^\dagger \times c_{d,\mathbf{p}+\mathbf{l}'}^\dagger c_{c,\mathbf{p}-\mathbf{q}} a_{\mathbf{l}'} c_{b,\mathbf{p}+\mathbf{k}} c_{a,\mathbf{p}} a_{\mathbf{k}} \quad (12)$$

or permutations $\mathbf{k}' \leftrightarrow \mathbf{l}'$, $\mathbf{k} \leftrightarrow \mathbf{l}$ for a total of four terms. Making the same assumption as before, this reduces to

$$n_{a,\mathbf{p}} n_{c,\mathbf{p}-\mathbf{q}} a_{\mathbf{l}'}^\dagger a_{\mathbf{k}'}^\dagger a_{\mathbf{l}} a_{\mathbf{k}}. \quad (13)$$

This process corresponds to the absorption of each photon by an atom before emission of either, and thus describes a two-atom process and is of the same order in the atomic number density as the Fermi and Bose corrections to single-atom scattering. The kinematical and geometric factors of Eq. (7) and Eq. (9) are the same for this process, and the resonance denominators are

$$\begin{aligned} R_1^{(2)} &= c(k+l-k') - \frac{\hbar}{M}[\mathbf{p} \cdot \mathbf{l}' + l'^2/2] - \omega_{da} + i\gamma_d \\ R_2^{(2)} &= c(k+l) - \frac{\hbar}{M}[\mathbf{p} \cdot \mathbf{k} + k^2/2 + (\mathbf{p}-\mathbf{q}) \cdot \mathbf{l} + l^2/2] \\ &\quad - \omega_{ba} + i\gamma_b - \omega_{dc} + i\gamma_d \\ R_3^{(2)} &= c(k) - \frac{\hbar}{M}[\mathbf{p} \cdot \mathbf{k} + k^2/2] - \omega_{ba} + i\gamma_b. \end{aligned} \quad (14)$$

Amplitudes for simultaneous scattering are shown in Fig. 6 for a gas with a phase space density of one half. Parameters are as for Fig. 2.

D. Fermi and Bose Gases

The statistical correction and two-atom scattering contributions add coherently, giving considerably different correlation functions for moderate degeneracy Bose vs. Fermi gases. This is illustrated in Fig. 7 and Fig. 8, which show the scattering rates vs. delay for Bose and Fermi gases with a phase space density of one half. Parameters are as for Fig. 2.

E. Ladder Process

In atoms with a "ladder" level structure, in which three levels $a-c$ are ordered in energy $\omega_c > \omega_b > \omega_a$ and connected by matrix elements $\mu_{ba}, \mu_{cb} \neq 0$, $\mu_{ca} = 0$, an additional process described by the diagram of Fig. 9 is possible. The relevant terms in $H'H'H'H'$ contain

$$\begin{aligned}
& c_{a,\mathbf{p}}^\dagger c_{d,\mathbf{p}+\mathbf{l}'} a_{\mathbf{l}'}^\dagger c_{d,\mathbf{p}+\mathbf{l}'}^\dagger c_{c,\mathbf{p}+\mathbf{k}+\mathbf{l}} a_{\mathbf{k}}^\dagger \\
& \times c_{c,\mathbf{p}+\mathbf{k}+\mathbf{l}}^\dagger c_{b,\mathbf{p}+\mathbf{k}} a_{\mathbf{l}} c_{b,\mathbf{p}+\mathbf{k}}^\dagger c_{a,\mathbf{p}} a_{\mathbf{k}}
\end{aligned} \tag{15}$$

or permutations $\mathbf{k}' \leftrightarrow \mathbf{l}'$, $\mathbf{k} \leftrightarrow \mathbf{l}$ for a total of four terms. Making the same assumption as before, this reduces to

$$n_{a,\mathbf{p}} a_{\mathbf{l}'}^\dagger a_{\mathbf{k}'}^\dagger a_{\mathbf{l}} a_{\mathbf{k}}. \tag{16}$$

This process corresponds to the absorption of both photons by an atom before emission of either, and thus describes a one-atom process which is of the same order in the atomic number density as one-atom scattering. The kinematical and geometric factors of Eq. (7) Eq. (9) are the same for this process, and the resonance denominators are

$$\begin{aligned}
R_1^{(3)} &= c(k+l-k') - \frac{\hbar}{M}[\mathbf{p} \cdot \mathbf{l}' + l'^2/2] - \omega_{da} + i\gamma_d \\
R_2^{(3)} &= c(k+l) - \frac{\hbar}{M}[\mathbf{p} \cdot (\mathbf{k} + \mathbf{l}) + |\mathbf{k} + \mathbf{l}|^2/2] \\
&\quad - \omega_{ca} + i\gamma_c \\
R_3^{(3)} &= c(k) - \frac{\hbar}{M}[\mathbf{p} \cdot \mathbf{k} + k^2/2] - \omega_{ba} + i\gamma_b.
\end{aligned} \tag{17}$$

Right-angle scattering amplitudes for this process are shown in Fig. 10. Parameters are as for Fig. 2.

F. Lorentz-model Behavior

It is interesting to consider the case of a ladder atom with equal energy spacing $\omega_{cb} = \omega_{ba}$ and matrix elements $|\mu_{cb}|^2 = 2|\mu_{ba}|^2$. In this case the states a - c are equivalent to the lowest three levels of a harmonic oscillator, i.e., to a Lorentz model, and the medium is effectively linear for two-photon processes.

The amplitudes for the one atom process of Eq. (4) and the ladder process of Eq. (15) partially cancel. The resulting signal is smaller and lacks oscillations, as shown in Fig. 11. Parameters are as for Fig. 2.

G. Background Events

In addition to the photon-photon scattering processes, Rayleigh scattering (and Raman scattering for more complicated atoms) will create an uncorrelated coincidence background. This background is calculated in Appendix A. The coincidence signal, consisting of both the Lorentz-model atom photon-photon scattering signal and the incoherent background is shown in Fig. 12. The peak coincidence rate (at $\delta\tau = 0$) is approximately twice the background, accidental coincidence rate. In the limit of large detuning, it becomes exactly twice accidental rate. This can be explained in analogy with the Hanbury-Brown-Twiss effect as follows: For the optimal geometry the drive beams are conjugates of each other $H(\mathbf{x}) = G^*(\mathbf{x})$ and the detectors are in opposite

directions. The linear atoms act to create a random index grating which scatters a chaotic but equal (up to phase conjugation) field to each detector. As expected for chaotic light [19], the fourth-order equal-time correlation function is twice the product of second-order correlation functions.

$$\langle E^2(\mathbf{x}_A, t) E^2(\mathbf{x}_B, t) \rangle = 2 \langle E^2(\mathbf{x}_A, t) \rangle \langle E^2(\mathbf{x}_B, t) \rangle. \tag{18}$$

IV. SMALL-ANGLE SCATTERING

Thus far the discussion has involved only large-angle scattering. In the context of cavity nonlinear optics all fields are propagating nearly along the optical axis of the cavity so it is necessary to consider scattering processes for nearly co-propagating or nearly counter-propagating photons. As argued above, the temporal width of the correlation signal scales as $1/q$, the inverse of the momentum transfer. This is shown in Fig. 13 and Fig. 14, which show rates for scattering photons from beams in the x - z plane into the y - z plane. In all cases the beam directions are 0.1 radian from the z axis. The coincidence distribution shows oscillations which die out on the time-scale of the inverse Doppler width, and a non-oscillating pedestal with a width determined by the momentum transfer q .

The pedestal, however, does not correspond to the duration of the nonlinear process in this case. As above, by considering a ladder atom with the energy spacings and matrix elements of a harmonic oscillator we can isolate the linear optical behavior. As shown in Fig. 15 and Fig. 16, this behavior includes the pedestal, but not the oscillations, indicating that the nonlinear optical process is still fast, with a time-scale on the order of the inverse Doppler width.

V. LIMITATIONS ON SCATTERING ANGLE

Due to the limited width of the atomic momentum distribution, the resonance denominator $R_2^{(1)}$ is small if the input and output photons are not of nearly the same energy. Since the complete process must conserve photon momentum, input photons with net transverse momentum in the output photon direction will scatter less strongly. The width of this resonance is very narrow: a net transverse momentum $k_y + l_y \sim k\sqrt{k_B T/Mc^2}$ is sufficient that few atoms will be resonant. As $\sqrt{k_B T/Mc^2}$ is typically of order 10^{-6} in an atomic vapor, this would be a severe restriction on the transverse momentum content of the beams in a cavity nonlinear optics experiment. However, as shown in Fig. 16, the narrow resonance associated with $R_2^{(1)}$ contributes the linear response of the medium. The nonlinear response, which has the same

resonance character as the “ladder” process, is not limited in this way because $R_2^{(3)}$ does not depend upon the output photon energies.

VI. OUTPUT POLARIZATION

The polarization of the output photons depends on the structure of the atom and can produce polarization-entangled photons. For example, if the input photons are propagating in the $\pm z$ directions and are x polarized, the two absorption events in the above diagram change the z component of angular momentum by $\delta m = \pm 1$. In order for the process to return the atom to its initial state, the two emission events must both produce $\delta m = \pm 1$ or both $\delta m = 0$. For right angle scattering with the detectors in the $\pm y$ directions, the output photons must therefore be either both x or both z polarized. If both polarizations are possible, the emitted photons are entangled in polarization, as well as in energy and in momentum.

VII. CONCLUSION

Time correlations in photon-photon scattering provide an indication of the time-scale over which the atomic medium is involved in the interaction among photons in a nonlinear medium. It is found that the time-scale is determined by the inhomogeneous broadening of the medium and the magnitude of the momentum transfer. For large-angle scattering, the time-scale of involvement is $\delta\tau \sim \Lambda M/\hbar q$, while for small-angle scattering the time-scale is $\delta\tau \sim \Lambda M/\hbar k$. As this time-scale is shorter than the atomic relaxation time, calculations which contain an adiabatic elimination of the atomic degrees of freedom necessarily overlook the fastest dynamics in this process.

APPENDIX A: PHOTON CORRELATIONS

1. Detection Amplitudes

Unlike a genuine two-body collision process, atom-mediated photon-photon scattering has a preferred reference frame which is determined by the atomic momentum distribution. To calculate the photon correlations we work in the “laboratory” frame and assume the momentum distribution is symmetric about zero. We consider scattering from two input beams with beam shapes $G(\mathbf{x}) \equiv V^{-1/2} \sum_{\mathbf{k}} g(\mathbf{k}) \exp[i\mathbf{k} \cdot \mathbf{x}]$ and $H(\mathbf{x}) \equiv V^{-1/2} \sum_{\mathbf{l}} h(\mathbf{l}) \exp[i\mathbf{l} \cdot \mathbf{x}]$ which are normalized as $\sum_{\mathbf{k}} |g(\mathbf{k})|^2 = \sum_{\mathbf{l}} |h(\mathbf{l})|^2 = 1$. We further assume that the beams are derived from the same monochromatic source and are paraxial, i.e., that $g(\mathbf{k})$ is only appreciable in some small neighborhood of the average beam direction \mathbf{k}_0 , and similarly for $h(\mathbf{l})$ around \mathbf{l}_0 . The geometry is shown schematically in Fig. 17. For convenience, the

beams are assumed to each contain one photon, so that the initial state of the field is

$$|\phi(0)\rangle = A_G^\dagger A_H^\dagger |0\rangle \quad (\text{A1})$$

where the creation operators A_G^\dagger, A_H^\dagger are $A_G^\dagger \equiv \sum_{\mathbf{k}} g(\mathbf{k}) a_{\mathbf{k}}^\dagger$ and $A_H^\dagger \equiv \sum_{\mathbf{l}} h(\mathbf{l}) a_{\mathbf{l}}^\dagger$. Scaling of the result to multiple photons is obvious.

We use Glauber photodetection theory to determine the rates at which scattering products arrive at two detectors A and B at space-time points (\mathbf{x}_A, t_A) and (\mathbf{x}_B, t_B) , respectively. We compute the correlation function in the Heisenberg representation

$$P(\mathbf{x}_A, t_A, \mathbf{x}_B, t_B) = |\langle 0 | \Phi_H^{(+)}(\mathbf{x}_B, t_B) \Phi_H^{(+)}(\mathbf{x}_A, t_A) | \phi(0) \rangle_H|^2 \quad (\text{A2})$$

where the photon field operator is

$$\Phi_H^{(+)}(\mathbf{x}, t) \equiv V^{-1/2} \sum_{\mathbf{k}, \alpha} a_{\mathbf{k}, \alpha}(t) \exp[i\mathbf{k} \cdot \mathbf{x}]. \quad (\text{A3})$$

This field operator is similar to the positive frequency part of the electric field and is chosen so that $\Phi^{(-)}(\mathbf{x}, t) \Phi^{(+)}(\mathbf{x}, t)$ is Mandel’s photon-density operator [20]. To make use of perturbation theory, Eq. (A2) is more conveniently expressed in interaction representation as

$$\begin{aligned} P(\mathbf{x}_A, t_A, \mathbf{x}_B, t_B) &= |\langle 0 | \Phi_I^{(+)}(\mathbf{x}_B, t_B) U_I(t_B, t_A) \Phi_I^{(+)}(\mathbf{x}_A, t_A) | \phi(t_A) \rangle_I|^2 \\ &= |\langle 0 | \Phi_I^{(+)}(\mathbf{x}_B, t_B) \Phi_I^{(+)}(\mathbf{x}_A, t_A) | \phi(t_A) \rangle_I|^2 \\ &\equiv |A(\mathbf{x}_A, t_A, \mathbf{x}_B, t_B)|^2 \end{aligned} \quad (\text{A4})$$

where U_I is the interaction picture time-evolution operator, the interaction picture field operator is

$$\Phi_I^{(+)}(\mathbf{x}, t) = V^{-1/2} \sum_{\mathbf{k}, \alpha} a_{\mathbf{k}, \alpha} \exp[i(\mathbf{k} \cdot \mathbf{x} - ckt)] \quad (\text{A5})$$

and in passing to the second line we have made the assumption that a detection at (\mathbf{x}_A, t_A) does not physically influence the behavior of photons at (\mathbf{x}_B, t_B) although there may be correlations. The the amplitude of joint detection is

$$\begin{aligned} A(\mathbf{x}_A, t_A, \mathbf{x}_B, t_B) &= \frac{(2\pi)^3}{V^2 \hbar} \sum_{\mathbf{k}, \mathbf{l}} \exp[i(\mathbf{k}' \cdot \mathbf{x}_A - ck't_A)] \\ &\quad \times \exp[i(\mathbf{l}' \cdot \mathbf{x}_B - cl't_B)] \\ &\quad \times \sum_{\mathbf{k}, \mathbf{l}} g(\mathbf{k}) h(\mathbf{l}) V_{\mathbf{l}' \mathbf{k}' \mathbf{l} \mathbf{k}} \\ &\quad \times \frac{1 - \exp[i(c(k' + l' - k - l)t_A)]}{c(k' + l' - k - l) + i\eta} \end{aligned} \quad (\text{A6})$$

Although $V_{\mathbf{l}'\mathbf{k}'\mathbf{l}\mathbf{k}}$ depends strongly upon the magnitudes of the initial and final photon momenta through the resonance denominators of Eq. (10), it depends only weakly on their directions through the geometrical factors of Eq. (9). This and the assumption of paraxial input beams justify the approximation

$$\begin{aligned} & \sum_{\mathbf{k}\mathbf{l}} g(\mathbf{k})h(\mathbf{l})V_{\mathbf{l}'\mathbf{k}'\mathbf{l}\mathbf{k}} \\ & \approx V_{\mathbf{l}'\mathbf{k}'\mathbf{l}_0\mathbf{k}_0} \sum_{\mathbf{k}\mathbf{l}} g(\mathbf{k})h(\mathbf{l})\delta_{\mathbf{k}+\mathbf{l},\mathbf{k}'+\mathbf{l}'} \\ & = V_{\mathbf{l}'\mathbf{k}'\mathbf{l}_0\mathbf{k}_0} \int d^3\mathbf{x}G(\mathbf{x})H(\mathbf{x}) \exp[-i(\mathbf{k}' + \mathbf{l}') \cdot \mathbf{x}]. \end{aligned} \quad (\text{A7})$$

We can similarly treat the output photons in the paraxial approximation for the case that the detection points are far from the interaction region, i.e., that $x_A, x_B \gg x$. Making these approximations and dropping unphysical portions of the solution propagating inward from the detectors toward the source region, we find

$$\begin{aligned} & A(\mathbf{x}_A, t_A, \mathbf{x}_B, t_B) \\ & = \frac{-i}{\hbar c} \int k' dk' l' V_{\mathbf{l}'\mathbf{k}'\mathbf{l}_0\mathbf{k}_0} \\ & \quad \times \int d^3\mathbf{x} \frac{G(\mathbf{x})H(\mathbf{x})}{|\mathbf{x}_A - \mathbf{x}||\mathbf{x}_B - \mathbf{x}|} \\ & \quad \times \exp[i(\mathbf{k}' \cdot (\mathbf{x}_A - \mathbf{x}) - ck't_A)] \\ & \quad \times \exp[i(\mathbf{l}' \cdot (\mathbf{x}_B - \mathbf{x}) - cl't_B)] \\ & \quad \times \theta(\tau_A)\theta(\tau_B) \end{aligned} \quad (\text{A8})$$

where $c\tau_{A,B} \equiv ct_{A,B} - x_{A,B}$ are retarded times.

A final approximation ignores the slow variation of k', l' relative to that of the resonant $V_{\mathbf{l}'\mathbf{k}'\mathbf{l}_0\mathbf{k}_0}$. Further, we define $G'(\mathbf{x}) \equiv G(\mathbf{x}) \exp[ik_0 \cdot \mathbf{x}]$, $H'(\mathbf{x}) \equiv H(\mathbf{x}) \exp[i\mathbf{l}_0 \cdot \mathbf{x}]$ and $k' \equiv k'_0 + \delta k'$ where \mathbf{k}'_0 is the value of \mathbf{k}' which maximizes $V_{\mathbf{l}'\mathbf{k}'\mathbf{l}_0\mathbf{k}_0}$ subject to momentum and energy conservation. This gives a simple expression for the correlation function

$$\begin{aligned} & A(\mathbf{x}_A, t_A, \mathbf{x}_B, t_B) \\ & = \frac{-ik'l'}{\hbar c} \exp[-ic(k'_0\tau_A + l'_0\tau_B)] \\ & \quad \times \int d\delta k' V_{\mathbf{l}'\mathbf{k}'\mathbf{l}_0\mathbf{k}_0} \exp[ic\delta k'(\tau_B - \tau_A)] \\ & \quad \times \int d^3\mathbf{x} \frac{G'(\mathbf{x})H'(\mathbf{x})}{|\mathbf{x}_A - \mathbf{x}||\mathbf{x}_B - \mathbf{x}|} \\ & \quad \times \exp[i(\mathbf{k}_0 + \mathbf{l}_0 - \mathbf{k}'_0 - \mathbf{l}'_0) \cdot \mathbf{x}] \\ & \quad \times \theta(\tau_A)\theta(\tau_B). \end{aligned} \quad (\text{A9})$$

This can be interpreted as consisting of a carrier wave, a Fourier transform of the scattering amplitude and a coherent integration of the contributions from different parts of the interaction region. The spatial integral enforces phase matching in the photon-photon scattering process.

2. Detection Rates

The probability for a coincidence detection at two detectors of specified area and in two specified time intervals is

$$P = \int d^2\mathbf{x}_A d^2\mathbf{x}_B c dt_A c dt_B |A(\mathbf{x}_A, t_A, \mathbf{x}_B, t_B)|^2, \quad (\text{A10})$$

where the integral is over the detector surfaces (each assumed normal to the line from scattering region to detector) and over the relevant time intervals. This is more conveniently expressed in terms of a rate W of coincidence detections in terms of the detector solid angles $\delta\Omega_A$, $\delta\Omega_B$ and the difference in retarded arrival times $\tau_- \equiv \tau_B - \tau_A$

$$W = c^2 x_A^2 x_B^2 |A(\mathbf{x}_A, t_A, \mathbf{x}_B, t_B)|^2 \delta\Omega_A \delta\Omega_B d\tau_-. \quad (\text{A11})$$

Coincidence rate is largest when the detectors are placed in the directions which satisfy the phase-matching condition. We assume that $\mathbf{k} + \mathbf{l} = \mathbf{k}' + \mathbf{l}' = 0$ and that the detectors are small compared to the source-detector distance, i.e., that $\delta\Omega_{A,B} \ll 1$. Under these conditions, the rate of coincidence events reduces to

$$\begin{aligned} W_{\text{scattering}} & = \frac{(k'l')^2}{\hbar^2} \left| \int d\delta k' V_{\mathbf{l}'\mathbf{k}'\mathbf{l}_0\mathbf{k}_0} \exp[ic\delta k' \tau_-] \right|^2 \\ & \quad \times \left| \int d^3\mathbf{x} G(\mathbf{x})H(\mathbf{x}) \right|^2 \delta\Omega_B \delta\Omega_B d\tau_-. \end{aligned} \quad (\text{A12})$$

3. Signal Contrast

In addition to the photon-photon scattering signal, uncorrelated Rayleigh and Raman scattering events give a background of accidental coincidences. The rate of scattering into a small solid angle $\delta\Omega$ is

$$W_{\text{BG}} = B\delta\Omega \int d^3x n_k \quad (\text{A13})$$

where

$$\begin{aligned} B & \equiv \sum_{a,c} \int d^3\mathbf{p} \langle n_{a,\mathbf{p}} \rangle (1 \pm \langle n_{c,\mathbf{p}'} \rangle) \frac{k_f^4 c}{(2\pi)^3 \hbar^2} \\ & \quad \times \left| \sum_b \frac{(\mathbf{e}_f \cdot \boldsymbol{\mu}_{bc})^* \mathbf{e}_i \cdot \boldsymbol{\mu}_{ba}}{ck + \omega_{ab} - \frac{\hbar}{M}[\mathbf{p} \cdot \mathbf{k} + k^2/2] + i\gamma_b} \right|^2 \end{aligned} \quad (\text{A14})$$

and n_k is the number density of photons propagating in the \mathbf{k} direction. In terms of the beam-shape functions for two colliding beams, the rate of accidental coincidences is

$$W_{\text{accidental}} = B^2 \left[\int d^3x |G(\mathbf{x})|^2 + |H(\mathbf{x})|^2 \right]^2 \times \delta\Omega_A \delta\Omega_B d\tau_- \quad (\text{A15})$$

The ratio of coincidences due to photon-photon scattering to accidental background coincidences is thus

$$\frac{W_{\text{scattering}}}{W_{\text{accidental}}} = \frac{(k'l')^2}{4\hbar^2} \frac{F}{B^2} \times \left| \int d\delta_{k'} V_{l'k'1_0k_0} \exp[ic\delta_{k'}\tau_-] \right|^2 \quad (\text{A16})$$

where F is the mode fidelity factor

$$F \equiv 4 \frac{[\int d^3x G(\mathbf{x})H(\mathbf{x})]^2}{[\int d^3x (|G(\mathbf{x})|^2 + |H(\mathbf{x})|^2)]^2} \quad (\text{A17})$$

-
- [1] J. Boyce and R. Chiao, *Physical Review A* **59**, 3953 (1999).
 [2] J. Boyce, J. P. Torres, and R. Y. Chiao, Submitted for publication (1999).
 [3] J. P. Torres, J. Boyce, and R. Y. Chiao, Submitted for publication (1999).
 [4] R. Y. Chiao, I. H. Deutsch, J. C. Garrison, and E. M. Wright, in *Frontiers in Nonlinear Optics, The Sergei Akhmanov Memorial Volume*, edited by H. Walther, N.

- Koroteev, and M. O. Scully (Institute of Physics Publishing, Bristol, 1992), pp. 151–182.
 [5] I. Deutsch, R. Chiao, and J. Garrison, *Physical Review Letters* **69**, 3627 (1992).
 [6] E. H. Lieb and W. Liniger, *Physical Review* **130**, 1605 (1963).
 [7] E. H. Lieb, *Physical Review* **130**, 1616 (1963).
 [8] P. Drummond and S. Carter, *Journal of the Optical Society of America B* **4**, 1565 (1987).
 [9] S. Carter, P. Drummond, M. Reid, and R. Shelby, *Physical Review Letters* **58**, 1841 (1987).
 [10] P. Drummond and M. Hillery, *Physical Review A* **59**, 691 (1999).
 [11] M. Hillery and L. Mlodinow, *Physical Review A* **30**, 1860 (1984).
 [12] P. Drummond, *Physical Review A* **42**, 6845 (1990).
 [13] I. Abram and E. Cohen, *Physical Review A* **44**, 500 (1991).
 [14] M. O. Scully and W. E. Lamb, Jr., *Physical Review* **159**, 208 (1967).
 [15] M. Sargent, III, D. Holm, and M. Zubairy, *Physical Review A* **31**, 3112 (1985).
 [16] P. Drummond and D. Walls, *Physical Review A* **23**, 2563 (1981).
 [17] W. H. Louisell, *Quantum Statistical Properties of Radiation*, *Wiley series in pure and applied optics* (John Wiley & Sons, New York, 1973).
 [18] A. Heidmann and S. Reynaud, *Journal of Modern Optics* **34**, 923 (1987).
 [19] D. F. Walls and G. J. Milburn, *Quantum Optics* (Springer, Berlin, 1994).
 [20] L. Mandel and E. Wolf, *Optical coherence and quantum optics* (Cambridge University Press, New York, 1995).

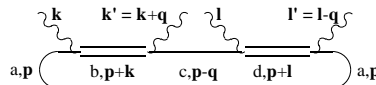


FIG. 1. Photon-photon scattering at a single atom.

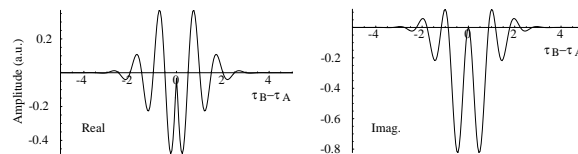


FIG. 2. Right-angle scattering amplitude A vs. time delay for the single-atom process of Fig. 1. The time unit is δ_D^{-1} .

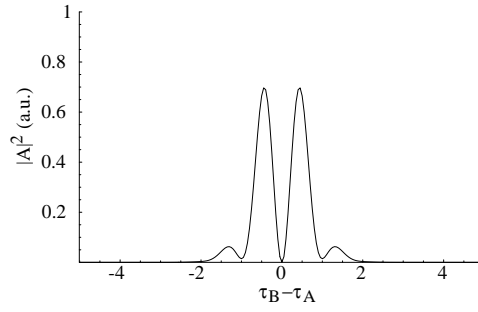


FIG. 3. FIG. 3. Right-angle scattering rate $|A|^2$ vs. time delay for the single-atom process of Fig. 1. Time unit is δ_D^{-1} .

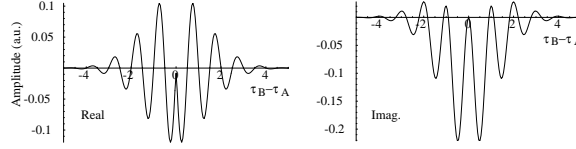


FIG. 4. FIG. 4. Statistical correction to the one-atom scattering amplitude. The time unit is δ_D^{-1} .

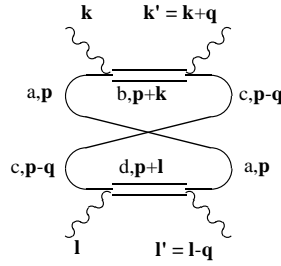


FIG. 5. FIG. 5. Two-atom photon-photon scattering.

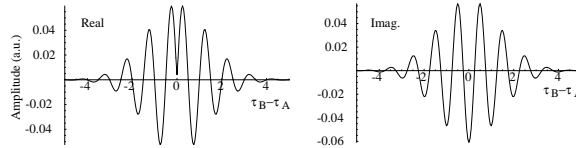


FIG. 6. FIG. 6. Scattering rate $|A|^2$ vs. time delay for the two-atom process of Fig. 5. The time unit is δ_D^{-1} .

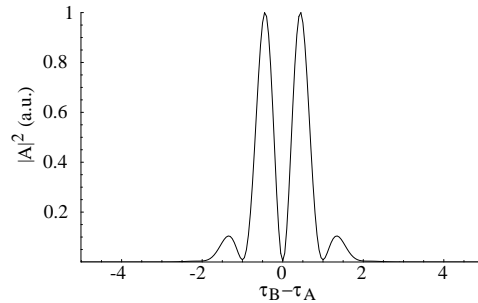


FIG. 7. FIG. 7. Scattering rate $|A|^2$ vs. time delay for a Bose gas of phase-space density $1/2$. The time unit is δ_D^{-1} .

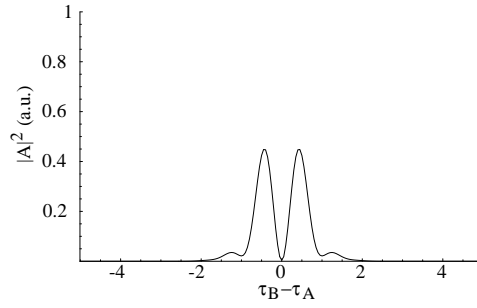


FIG. 8. FIG. 8. Scattering rate $|A|^2$ vs. time delay for a Fermi gas of phase-space density $1/2$. The time unit is δ_D^{-1} .

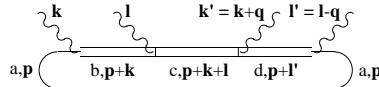


FIG. 9. FIG. 9. “Ladder” process in a three-level atom.

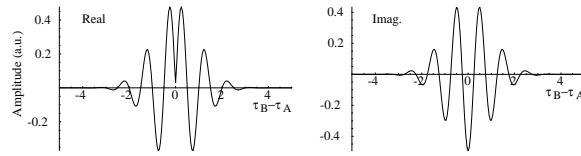


FIG. 10. FIG. 10. Scattering rate $|A|^2$ vs. time delay for the “ladder” process of Fig. 9. The time unit is δ_D^{-1} .

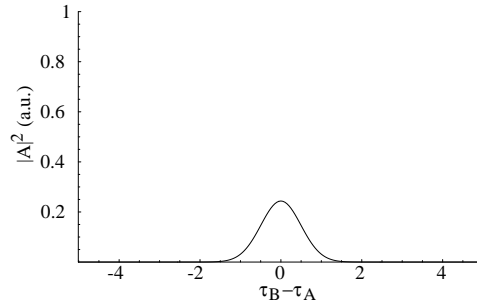


FIG. 11. FIG. 11. Scattering rate $|A|^2$ vs. time delay for a Lorentz-model atomic medium. The time unit is δ_D^{-1} .

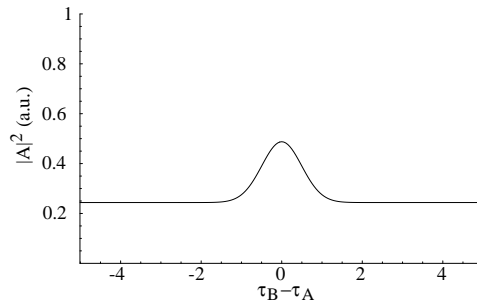


FIG. 12. FIG. 12. Coincidence rate vs. time delay for a Lorentz-model atomic medium. The constant background is accidental coincidences due to independent Rayleigh scattering events. The time unit is δ_D^{-1} .

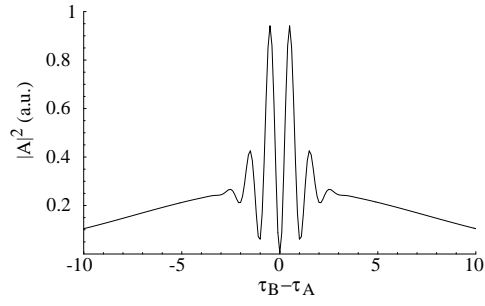


FIG. 13. FIG. 13. Small angle scattering rate $|A|^2$ vs. time delay for nearly co-propagating photons. Time unit is δ_D^{-1} .

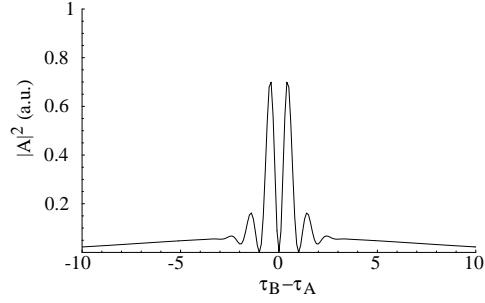


FIG. 14. FIG. 14. Right-angle scattering rate $|A|^2$ vs. time delay for nearly counter-propagating photons. Time unit is δ_D^{-1} .

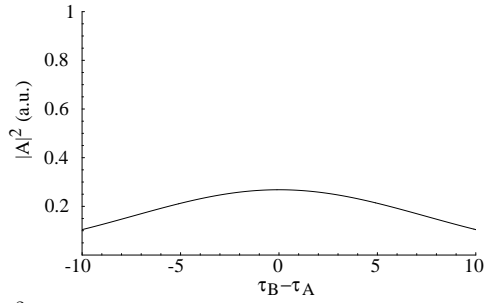


FIG. 15. FIG. 15. Coincidence rate $|A|^2$ vs. time delay for nearly co-propagating photons in a linear medium. $\gamma_b = 0.01\delta_D$, $\Delta = 2\pi\delta_D$. Time unit is δ_D^{-1} .

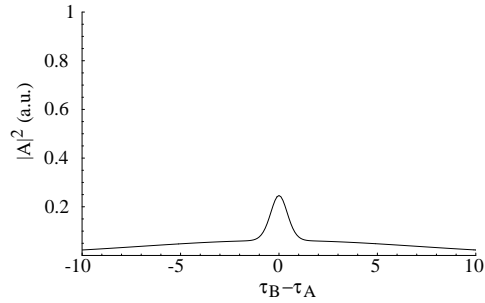


FIG. 16. FIG. 16. Coincidence rate $|A|^2$ vs. time delay for nearly counter-propagating photons linear medium. $\gamma_b = 0.01\delta_D$, $\Delta = 2\pi\delta_D$. Time unit is δ_D^{-1} .

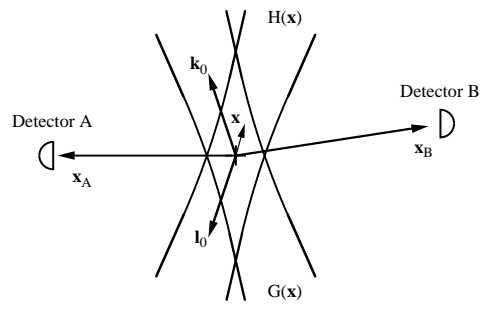


FIG. 17. FIG. 17. Geometry of collision process.